Target residues from the interaction of copper with 15–45 MeV/nucleon ^{12}C ions

S. Y. Cho and N. T. Porile
Department of Chemistry, Purdue University, West Lafayette, Indiana 47907

D. J. Morrissey
National Superconducting Cyclotron Laboratory, Michigan State University, East Lansing, Michigan 48824
(Received 27 December 1988)

Target residues from the interaction of copper with 15, 25, and 45 MeV/nucleon ^{12}C ions have been studied by off-line γ-ray spectroscopy. Cross sections, average ranges, and forward-to-backward ratios were measured for some 35 products. The data were used to obtain the isobaric yield distribution, the mass yield distribution, the mean longitudinal momentum transfer, and the mean excitation energy. The evolution of these quantities with energy is examined in conjunction with our previous results for 35 MeV/nucleon ^{12}C ions.

I. INTRODUCTION

The recent availability of intermediate energy heavy ions has made it possible to investigate the transition between nuclear reaction mechanisms dominated by mean field dynamics and those dominated by nucleon-nucleon interactions. The study of target fragmentation residues in heavy-ion reactions constitutes one of the approaches that can provide information on the evolution of the dynamics. For example, experiments on target fragmentation residues can be used to study the energy dependence of the longitudinal momentum transfer and of the mass yield distribution, as well as the onset of intermediate-mass fragment production and its energy dependence. These results have typically been obtained by means of cross section and recoil range measurements involving off-line γ-ray spectrometry to detect the reaction products.

The most complete measurements of this type have been reported for the interaction of copper with ^{12}C ions, where cross section and recoil data are available at relativistic energies,[1–5] at 86A MeV (Ref. 6–8) and 35A MeV,[9] and recoil data only have been reported for 22A and 84A MeV ^{12}C ions.[10] The most striking changes occur at the lowest energies, where complete fusion gives way to incomplete fusion. We report here the results of cross section and recoil measurements for target residues of the interaction of copper with 15–45A MeV ^{12}C ions. A preliminary report of the results has been given elsewhere.[11]

II. EXPERIMENTAL

The experiment was performed at the K 500 cyclotron of the National Superconducting Laboratory (NSCL) at Michigan State University. The experimental procedure has been described in detail in a previous publication.[9] Briefly, target stacks consisting of a 20.7 mg/cm^2 copper foil surrounded by 10-mg/cm^2-thick Mylar forward and backward catcher foils were irradiated with ^{12}C ions in a vacuum. The energies of the incident ^{12}C ions were 15A, 25A, and 45A MeV. The energies at the center of the targets were reduced to 151, 280, and 528 MeV, respectively, owing to the energy loss in Mylar and copper.[12] Irradiations were either 0.5 or 3.5 h long. The beam intensity varied between 10 and 20 ena, as determined with a Faraday cup.

Because of the substantial production of sodium isotopes in Mylar at 15A MeV, the experiment at this energy was repeated with 10.8-mg/cm^2-thick carbon foils replacing the Mylar catchers. This irradiation was performed at Argonne National Laboratory using the ATLAS facility. The direct production of sodium isotopes in Mylar at the higher energies was of minor importance and the activation contribution was determined by means of additional Mylar foils placed next to the catcher foils in the target stack.

Following the irradiations, the various foils were assayed with calibrated Ge(Li) or intrinsic Ge γ-ray spectrometers. The samples from the short irradiations were assayed at NSCL for approximately 1 d. Those from the long irradiations were assayed at Purdue University starting 1 d following irradiation and continuing for several months. The samples from the ATLAS irradiation were assayed at Purdue, beginning several hours after the end of bombardment. The intensities of $\sim$120 γ rays were determined with the code SAMPO,[13] and decay curves were analyzed with the CLSQ code.[14] Nuclidic assignments were made on the basis of energy, half-life, and concordance with other γ rays emitted by a presumed nuclide.[15]

III. RESULTS

The cross sections measured in this work are summarized in Table I, where each value is the weighted average of as many as nine separate determinations (two irradiations, several γ rays). The tabulated uncertainties are the larger of the standard deviation in the mean value and the estimated uncertainty of the individual determinations. The latter are based on the propagation of the errors in the SAMPO and CLSQ fits and, in addition, include

TABLE I. Cross sections for the production of target residues in the interaction of copper with ^{12}C ions.

Nuclide	Type	Energy σ (mb)	15A MeV	25A MeV	45A MeV
^{22}Na	C^+			1.52±0.23	1.32±0.15
^{24}Na	C^-		1.12±0.19	1.14±0.13	1.70±0.17
^{28}Mg	C^-		0.05±0.00	0.07±0.01	0.17±0.01
$^{34}Cl^m$	C^+			0.16±0.05	0.49±0.07
^{39}Cl	C^-				0.30±0.03
^{41}Ar	C^-			0.12±0.03	0.66±0.07
^{42}K	I			1.23±0.14	4.51±0.46
^{43}K	C^-		0.19±0.06	0.30±0.02	1.30±0.07
^{44}Sc	I			0.88±0.09	5.36±0.81
$^{44}Sc^m$	I		0.42±0.08	3.46±0.35	12.1±1.3
^{46}Sc	I		0.82±0.12	4.36±0.22	13.4±0.7
^{47}Sc	I		0.48±0.05	1.86±0.19	5.25±0.53
^{48}Sc	I			0.25±0.05	0.74±0.14
^{48}V	C^+		0.87±0.04	11.0±0.6	24.4±1.4
^{48}Cr	C^+			0.20±0.03	0.68±0.05
^{49}Cr	C^+		0.69±0.19	2.52±0.27	6.05±0.66
^{51}Cr	C^+		3.68±0.63	53.3±14.0	71.4±7.2
^{52}Mn	I		1.14±0.07	22.3±1.3	23.7±1.6
$^{52}Mn^m$	C^+			2.15±0.24	3.97±0.52
^{54}Mn	I		9.34±1.00	71.4±7.2	59.6±6.0
^{55}Co	C^+		0.17±0.05	3.63±0.23	2.56±0.28
^{56}Mn	C^-		0.69±0.05	6.22±0.36	5.75±0.31
^{56}Co	C^+		3.94±0.30	29.4±1.6	19.4±1.2
^{57}Co	C^+		28.8±4.5	115±9	68.9±4.3
^{57}Ni	C^+		0.26±0.03	2.87±0.15	1.93±0.11
^{58}Co	I		43.2±12.4	134±11	74.3±6.1
^{59}Fe	C^-		0.75±0.09	2.95±0.15	2.86±0.15
^{60}Co	I		13.1±1.0	26.9±4.0	19.2±1.0
^{60}Cu	C^+		5.96±0.32	16.3±1.0	8.41±0.51
^{61}Co	C^-			5.40±0.30	3.54±0.39
^{61}Cu	C^+		49.1±2.7	64.0±6.4	33.2±3.0
^{62}Zn	C^+		11.1±0.8	11.9±1.3	3.80±0.26
^{63}Zn	C^+		63.1±9.6	46.4±3.0	13.1±0.9
^{64}Cu	I		102±9		60.9±3.8
^{65}Zn	C^+		188±21	74.2±7.4	14.3±1.4
^{66}Ga	C^+		114±10	34.8±0.8	
^{67}Ga	C^+		129±7	30.2±0.8	

a 5% uncertainty in detector efficiencies. An additional 5% uncertainty has been folded into the overall uncertainty of cross sections based on a single determination of a single γ ray. The cross sections for ^{24}Na and ^{22}Na production have been reduced by 2–7 % in order to correct for the direct production of these products in the Mylar or carbon catchers.

The products listed in Table I have been identified with respect to their cumulation of the isobaric yield. Nuclides whose measured cross section includes those of more neutron-rich isobaric progenitors are labeled C^-, those having cross sections that include the yields of more proton-rich isobaric progenitors are labeled C^+, and those with no isobaric feed-in are labeled I (independent yields).

The various products can be grouped into three categories on the basis of the energy dependence of their cross sections. Products with $A \lesssim 50$ have cross sections that increase monotonically with energy in the regime of interest. Products with $A \sim 51-62$ have cross sections that peak between 15A and 45A MeV. Finally, products that lie very close in mass to the target have cross sections that decrease with increasing energy. Some typical excitation functions are shown in Fig. 1. Our earlier data[9] for 35A MeV ^{12}C ions are included.

The results of the recoil measurements can be expressed in terms of the average forward range, FW, and the ratio of forward-to-backward emission, F/B. The quantities F and B are the fractions of the total activity of a given nuclide collected in the forward and backward catchers, respectively, and W is the target thickness. The data are summarized in Table II. The tabulated uncertainties were determined in a similar manner as those in the cross sections. The ranges of ^{24}Na and ^{22}Na were reduced by 1–7 % to correct for the direct production in Mylar or carbon. The F/B values are large at all ener-

TABLE II. Recoil properties of products of the interaction of copper with ^{12}C ions.

	15 A MeV		25 A MeV		45 A MeV	
Nuclide	FW (mg/cm^2)	F/B	FW (mg/cm^2)	F/B	FW (mg/cm^2)	F/B
$^{22}Na^a$			7.95±1.35		5.80±0.69	
$^{24}Na^a$	5.77±0.68		5.02±0.51	> 17	5.02±0.51	
^{28}Mg	2.09±0.47		4.01±1.54		4.00±0.57	
$^{34}Cl^m$			4.04±1.85	> 2.5	4.47±0.68	> 5
^{42}K			2.82±0.37	> 9	2.73±0.29	
^{43}K	3.52±0.58		2.61±0.29		2.27±0.23	> 6
^{44}Sc			2.42±0.29	> 29	1.25±0.14	
$^{44}Sc^m$	2.78±0.35	> 3.9	2.54±0.26	138±45	2.40±0.25	332±51
^{46}Sc	1.27±0.17		2.52±0.26	> 43	2.29±0.23	73±24
^{47}Sc	2.15±0.26		2.55±0.26	192±18	2.26±0.23	177±59
^{48}Sc			3.54±0.48	> 37	2.21±0.23	
^{48}V	1.84±0.19		2.41±0.24		2.21±0.22	439±40
^{48}Cr			2.01±0.33	51±16	2.27±0.23	146±30
^{49}Cr			2.32±0.45	> 10	1.53±0.38	> 56
^{51}Cr	1.57±0.19		2.35±0.25		2.06±0.21	352±72
^{52}Mn	1.52±0.16		2.44±0.25	> 85	2.09±0.21	524±39
^{52}Fe			2.10±0.24	56±12	1.92±0.21	
^{54}Mn	1.61±0.18		2.43±0.25		1.84±0.19	> 266
^{55}Co			2.30±0.23	> 9	1.75±0.20	> 10
^{56}Mn	2.91±0.58		2.41±0.24	> 8.6	1.52±0.66	
^{56}Co	1.39±0.21		2.28±0.23		1.57±0.16	
^{57}Co	1.15±0.12		2.22±0.22	984±386	1.37±0.14	227±42
^{57}Ni	1.80±0.41		2.17±0.22		1.42±0.16	> 5
^{58}Co	1.47±0.18		2.11±0.22		1.19±0.12	183±35
^{59}Fe	1.07±0.11		1.98±0.20	> 68	1.00±0.10	
^{60}Co	1.58±0.19		1.89±0.26	95±14	1.06±0.13	
^{60}Cu	1.40±0.18					
^{61}Co			1.28±0.14		0.92±0.10	38±13
^{61}Cu	1.41±0.16	> 27	1.73±0.17	> 16	0.68±0.07	> 23
^{62}Zn	2.00±0.28		1.83±0.20	> 13	0.73±0.09	
^{63}Zn	1.96±0.40					
^{65}Zn	2.24±0.27		1.55±0.16		0.59±0.07	

[a]The $v_{\parallel}$ values associated with the formation of Na nuclides were obtained using the method of Winsberg. (Ref. 32). We used measured or estimated lower limits of F/B as input for this analysis. For these large F/B values, the results are insensitive to the actual values of F/B.

gies; in many cases only lower limits are given. The energy dependence of the FW values varies from product to product and is best examined once the longitudinal momentum transfer is obtained.

IV. DISCUSSION

A. Isobaric yield distribution

The measured cross sections account for only a fraction of the total mass yield. In order to obtain the isobaric and mass yield distributions it is necessary to estimate the cross sections of unmeasured nuclides. To do so, we use a generalization of the Rudstam formula,[16] which assumes an exponential mass yield distribution and a Gaussian isobaric yield distribution. As discussed in previous reports from our group,[9,17] cross sections of reactions induced by intermediate-energy and relativistic heavy ions are well represented by the following ten-parameter formula:

$$\sigma(Z,A)=\exp[\alpha_1+\alpha_2 A+\alpha_3 A^2+\alpha_4 A^3 + (\alpha_5+\alpha_6 A+\alpha_7 A^2)|Z_p-Z|^{\alpha_8}] . \quad (1)$$

The parameters α_1–α_4 determine the shape of the mass yield distribution, which is represented as an exponential in powers of A, with terms up to A^3. The parameters α_5–α_7 determine the width of the isobaric yield distribution. The inclusion of the two A-dependent terms allows for a possible mass dependence in the width. The parameter α_8 determines the shape of the isobaric yield distribution at a given mass number, where $\alpha_8=2$ corresponds to a Gaussian distribution. The isobaric yield distribution is assumed to be symmetric about the most probable charge Z_p, whose dependence on mass is parametrized as

$$Z_p=\alpha_9 A+\alpha_{10} A^2 . \quad (2)$$

The measured cross sections were fitted with Eq. (1) by means of an iterative least-squares code.[18] In the first

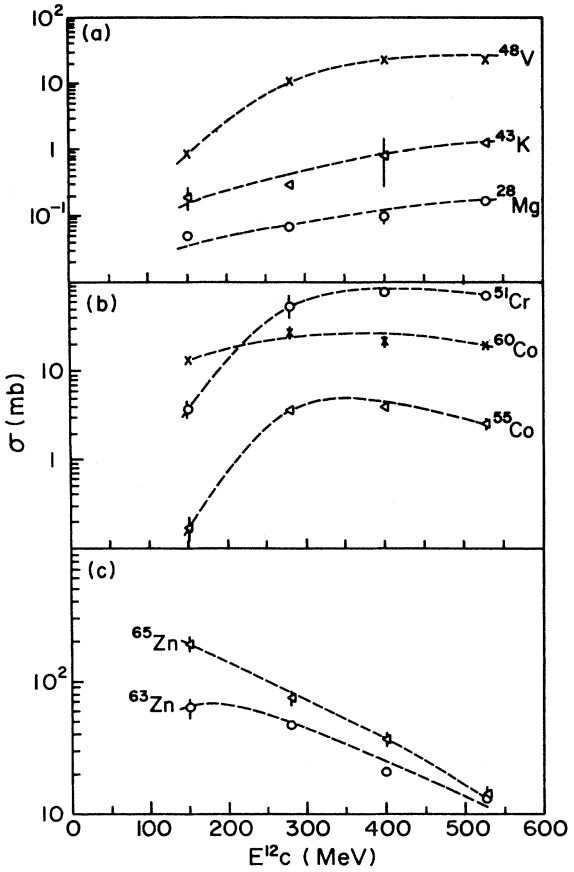

FIG. 1. Excitation functions for (a) low-mass, (b) intermediate-mass, and (c) high-mass products of the interaction of copper with ^{12}C ions.

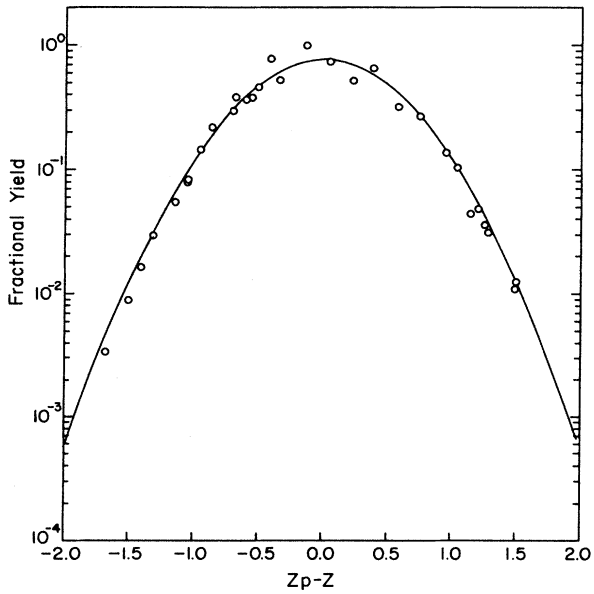

FIG. 2. Fractional isobaric yield distribution for the interaction of copper with 25A MeV ^{12}C ions. Curve: fitted values at $A=51$; circles: data scaled to $A=51$.

iteration, Eq. (1) was fitted to both cumulative and independent yields. The cumulative cross sections were then corrected for isobaric feed-in by means of the calculated progenitor cross sections and the resulting independent yields were refitted. It was found that this procedure converged after some three iterations. The values of $\alpha_1-\alpha_{10}$ are given in Table III.

A typical comparison of the fitted isobaric yield distribution with the data is shown in Fig. 2. In order to compare the independent yields derived from the measured cross sections with the isobaric yield distribution, it is convenient to divide both the corrected experimental cross sections as well as the calculated cross sections by the calculated total isobaric cross section in order to obtain fractional isobaric yields, F. For display purposes, the experimental values of F are scaled to a common mass number, $A=51$, using the ratio of calculated F values at $A=51$ and at the mass number in question as the scaling factor. Figure 2 shows that the parametrization provides a good fit to the isobaric yield distribution obtained at 25A MeV. Comparable fits are obtained at the other energies.

The evolution of the isobaric yield distribution with energy is examined in Fig. 3. Our results for 35A MeV ^{12}C are included.[9] Within the limits of uncertainly, both the full width at half maximum (FWHM) and Z_p are approximately independent of energy. While the figure shows

TABLE III. Parameters obtained from the fit of Eq. (1) to the cross sections of products from the interaction of copper with 15–45A MeV ^{12}C ions.

Parameter	Energy 15A MeV	25A MeV	45A MeV
α_1	122.4±2.5	27.2±0.3	15.5±0.2
α_2	−7.41±0.14	−2.25±0.02	−1.35±0.02
α_3	(14.4±0.2)×10^{-2}	(5.63±0.25)×10^{-2}	(3.74±0.04)×10^{-2}
α_4	−(8.90±0.14)×10^{-4}	−(4.19±0.04)×10^{-4}	−(3.01±0.04)×10^{-4}
α_5	19.9±0.4	2.02±0.11	0.30±0.11
α_6	−0.76±0.02	−0.17±0.00	−(9.23±0.49)×10^{-2}
α_7	(6.60±0.13)×10^{-3}	(1.71±0.05)×10^{-3}	(9.90±0.53)×10^{-4}
α_8	2.30±0.02	1.94±0.01	1.88±0.01
α_9	0.48±0.00	0.48±0.00	0.48±0.00
α_{10}	−(2.89±0.06)×10^{-4}	−(2.38±0.04)×10^{-4}	−(2.52±0.03)×10^{-4}

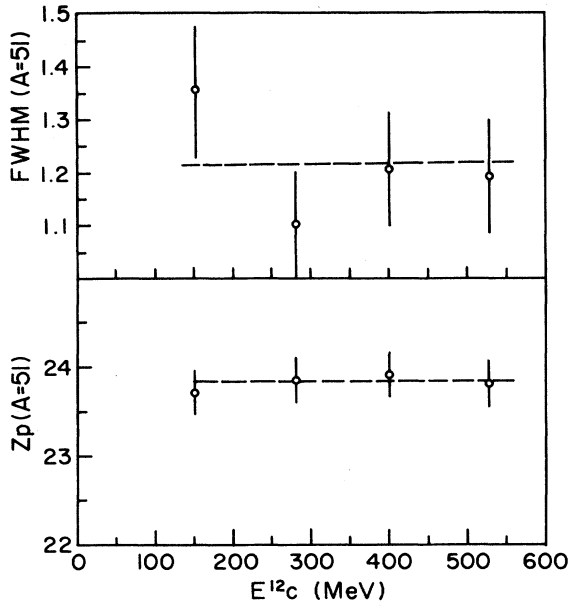

FIG. 3. Energy dependence of the full width at half maximum (top panel), and of Z_p (bottom), evaluated at $A=51$.

the results at $A=51$, similar results are also obtained at other mass numbers.

B. Mass yield distribution

Equation (1) may be used to evaluate the cross sections of unmeasured nuclides. These cross sections were added to the experimental yields at the same mass number in order to obtain the experimental mass yield distribution. A 20% uncertainty in the calculated yields has been folded into the overall uncertainty of each total isobaric yield. The resulting mass yield distributions are shown in Fig. 4. The curves through the data represent the total isobaric cross sections at each mass number obtained by means of Eq. (1). It is seen that the parametrization provides a good fit to the data.

The evolution of the mass yield distribution with energy is shown in Fig. 5, which includes the results obtained at 35A MeV (Ref. 9) and at 86A MeV.[7] With increasing energy, the curves broaden and the peak in the distribution moves to lower mass numbers. The mass yield distribution obtained at 15A MeV is unique in that the highest yields are obtained for transtarget products. This result suggests that complete or near-complete fusion must be important at this energy.

The mass yield distributions go through a minimum at $A\sim30$–35. The depth of this minimum decreases with increasing energy. Thus products with masses below this minimum ($A<30$) already have significant cross sections at the lowest energy. These observations are consistent with a change in mechanism whereby products with $A\gtrsim35$ are formed by spallation and those with $A\lesssim30$ are formed in a binary breakup process, as substantiated by coincidence measurements.[19] The results displayed in Fig. 5 may be quantified further by evaluation of the

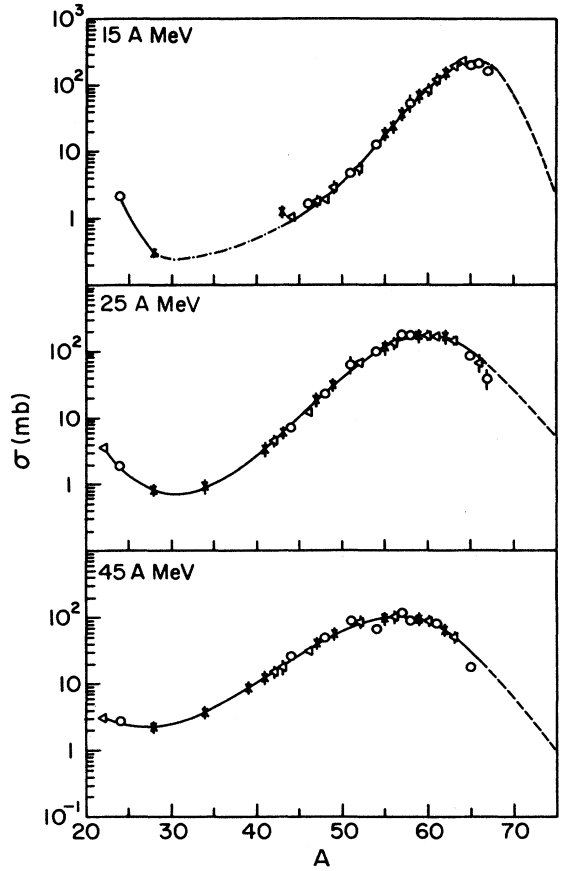

FIG. 4. Mass yield distributions for the interaction of copper with 15–45A MeV ^{12}C ions. Curves, Eq. (1) parametrization. Points, experimental cross sections corrected for unmeasured yields. The different symbols indicate the fraction of each yield that was measured: ○, >50%; △ 20–50%; × <20%. The dot-dashed part of the 15A MeV curve represents an interpolation between data points. The dashed curves are extrapolations to $A=75$.

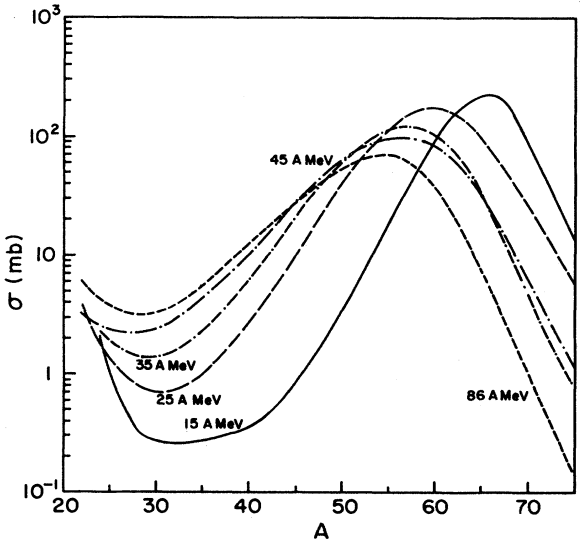

FIG. 5. Variation of the mass yield distribution with ^{12}C energy.

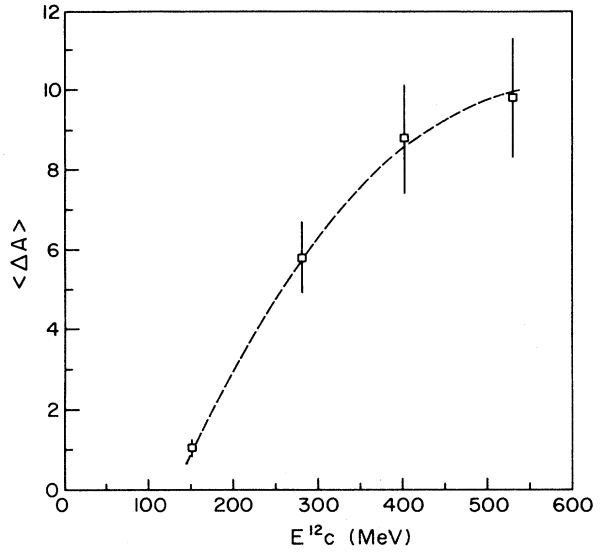

FIG. 6. Mean mass loss $\langle \Delta A \rangle$ from target ($A=64$) as a function of ^{12}C energy.

mean mass loss from the $A=64$ target. This is not the *actual* mass loss since, as shown in Sec. IV D, the composite system has $A>64$. The results are shown in Fig. 6, where the error bars denote the standard deviations in the mass loss distributions. The mean mass loss increases from approximately 1 to 10 u over the energy range of interest, with the increase being most pronounced at the lowest energies.

Over much of the mass interval, the mass yield distributions vary exponentially. Cumming *et al.*[20] have examined the energy dependence of the slope of this exponential region for a variety of projectiles interacting with copper. Figure 7 shows the slopes extracted from our data along with the results summarized by Cumming *et al.*[20] The present data lie in the energy regime in which the slope decreases with increasing energy and agree well with the Cumming systematics. Since in the energy regime of present interest these systematics are based on light-ion data, this agreement supports the notion that the deexcitation process depends on the total projectile energy but not on projectile identity (factorization).

C. Total reaction cross sections

The mass yield distributions may be integrated over mass in order to obtain the total reaction cross section σ_R at each energy. The integration was carried out over the $A=28-75$ mass range, where an extrapolation was performed above $A=68$. This extrapolation was of significance at the lowest energies, where transtarget yields are high. Products with $A<28$ were excluded on the presumption that they have detectable partners with $A>28$. The results are displayed in Fig. 8. The values of σ_R are in the vicinity of $2b$ and appear to peak at ~ 300 MeV.

Figure 8 also shows the result of a calculation of σ_R based on the parametrization of Kox *et al.*,[21] which incorporates the physical content of Karol's microscopic model.[22] The parameters used by Kox were fixed by fitting heavy-ion σ_R data, determined primarily by direct attenuation measurements. The calculated values are as much as 25% higher than the present results, the largest discrepancy occurring at the highest energy. This discrepancy, which has been cited previously,[9] suggests that our technique may miss some of the cross section. The two likeliest possibilities are (1) interactions in which

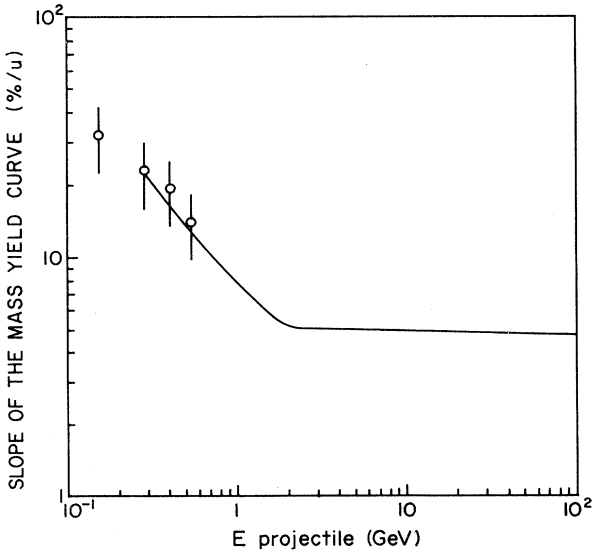

FIG. 7. Slope of the exponential region of the Cu mass yield curve versus projectile energy. Circles: present data and Ref. 9; curve: from Ref. 20.

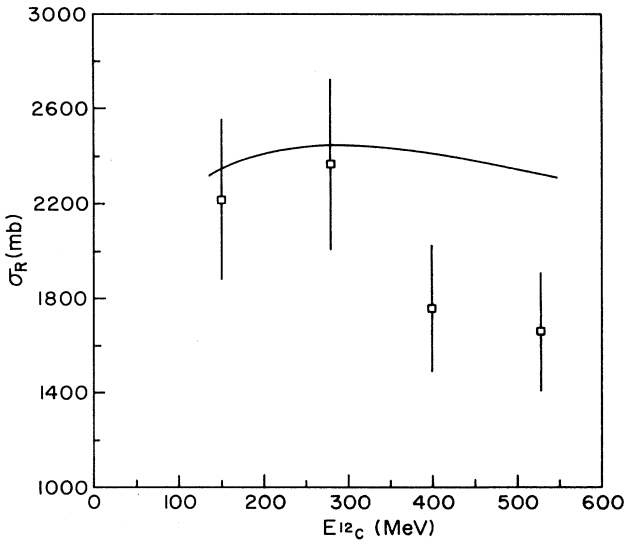

FIG. 8. Energy dependence of the total reaction cross section σ_R. The solid curve is based on the parametrization of Kox *et al.* (Ref. 21).

the target breaks up into fragments none of which have $A \geq 28$, and (2) interactions populating very specific final states, e.g., bound excited states of the target nucleus, to a substantially larger extent than predicted by our cross-section parametrization.

Although the present values of σ_R are smaller than those of Kox *et al.*,[21] they resemble them in showing a peak at ~ 300 MeV, albeit with a sizeable uncertainty. According to the model, this peak reflects the occurrence of two opposing factors: (1) the Coulomb barrier reduces σ_R at low energies, and (2) surface transparency, resulting from an increase with energy in the nucleon mean free path, reduces σ_R at high energies.

D. Longitudinal momentum transfer

The mean longitudinal velocity component $v_\parallel$ acquired by the struck nucleus in its interaction with ^{12}C was obtained from the recoil data in the manner discussed in detail in a previous report.[9] A different value is obtained from the data for each product. The results are shown in Fig. 9 as the variation with mass loss from the target of the ratio of $v_\parallel$ to v_{CN}, the velocity of the putative compound nucleus. At a given energy, the values of $v_\parallel/v_{CN}$ increase with the mass loss, although at $15A$ MeV the values are almost uniformly close to unity. For a given mass loss, the values of $v_\parallel/v_{CN}$ decrease with increasing energy showing that complete fusion gives way to increasingly incomplete fusion.

The results shown in Fig. 9 may be examined in terms of a model that has been applied to peripheral reactions at high energies. Cumming[4,10,23] has shown that when such reactions were treated as quasi-two-body processes, the longitudinal momentum of the composite system, $p_\parallel$, is related to the energy transferred to this system, ΔE, the main component of which is the excitation energy of the system, as

$$p_\parallel = \Delta E[1+k(1-\beta^2)^{1/2}]/\beta \ , \tag{3}$$

where the parameter k determines how rapidly $p_\parallel$ increases above its asymptotic value, ΔE, as the projectile velocity, β, decreases. It has been found[4] that target fragmentation reactions of copper are consistent with $k \sim 1$.

The dashed lines in Fig. 9 have been obtained by means of Eq. (3) using experimental values of ΔE determined at high energies[4] and $k=1$. The model predicts the observed increase of $v_\parallel/v_{CN}$ with ΔA up to compound nucleus values of $v_\parallel$, which is a consequence of the proportionality between $p_\parallel$ and ΔE in Eq. (1). However, the calculated velocities are consistently lower than the experimental values, with the deviations becoming particularly large at the lower energies, particularly for products close in mass to the target. These large deviations presumably are a consequence of the onset of typical low-energy processes, such as compound nucleus formation or deep inelastic reactions.[10]

The values of $v_\parallel$ can be interpreted in terms of a commonly used model,[24] which pictures the initial interaction as involving incomplete fusion, with beam velocity particles of total mass Δm escaping at 0°. Figure 10 shows the

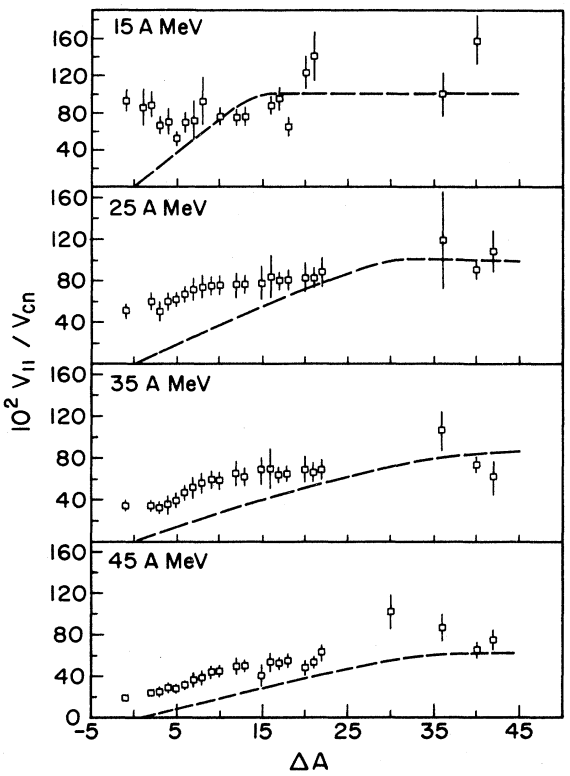

FIG. 9. Variation with mass loss from the target, ΔA, of the fractional velocity transfer in the interaction of copper with 15–45A MeV. The dashed curves show the prediction of a high-energy quasi-two-body model.

energy dependence of the mean values of Δm, averaged over the mass yield distribution. The values of $\langle \Delta m \rangle$ increase linearly with energy in the regime of interest. At the lowest energy, the composite system is, on average, only 2 mass units lighter than the compound nucleus while at the highest energy only an α particle is, on aver-

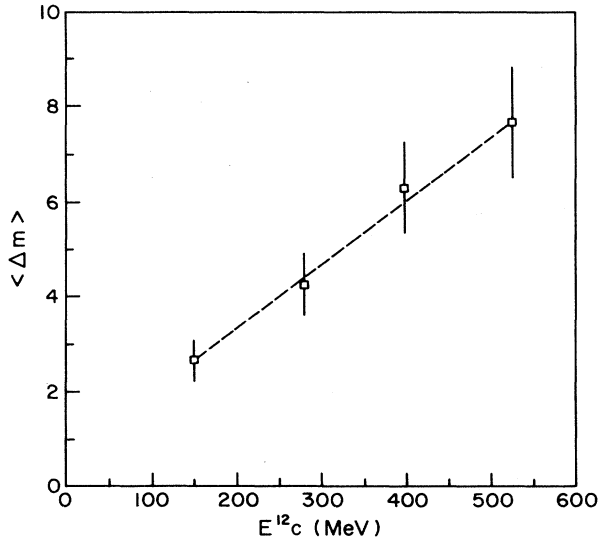

FIG. 10. Energy dependence of $\langle \Delta m \rangle$, the mean mass loss in the initial interaction.

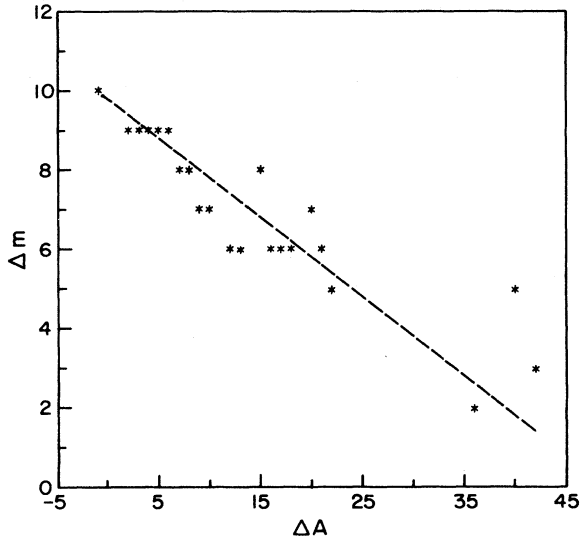

FIG. 11. Variation of Δm with ΔA for 45 A MeV ^{12}C ions.

age, transferred to the target in the initial interaction. At a given energy, the values of Δm decrease with increasing mass loss, as illustrated in Fig. 11. As in relativistic interactions, this behavior is suggestive of a geometric origin, with products close to the target formed in peripheral interactions and those of low mass formed in more central collisions.

The values of Δm permit a determination of the mass of the composite system. When combined with the values of $v_{\parallel}$, the longitudinal momentum transfer (LMT) is obtained. The mean LMT, obtained by weighting the individual LMT values by the respective isobaric cross sections, is plotted as a function of energy in Fig. 12. The mean LMT attains a maximum value of approximately 1.7 GeV/c for 25 A MeV ^{12}C and decreases at higher energies. This behavior is the result of two opposing trends: the increase in the initial projectile momentum and the decrease in the fractional LMT. The maximum LMT is somewhat lower than the limiting value of 175 MeV/c per projectile nucleon derived by Leray[24] from data in the literature.

The decrease in the fractional LMT with increasing projectile energy has been found to be nearly independent of projectile and target mass.[24–26] Leray[24] has shown that this decrease is nearly linear in the relative velocity

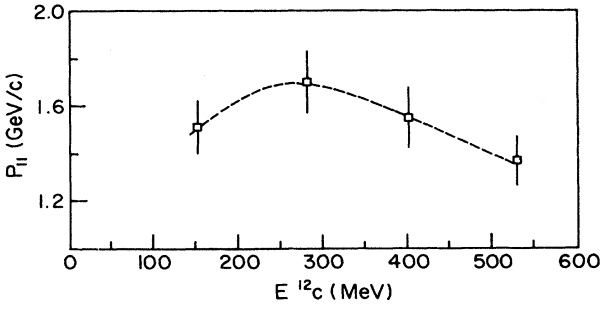

FIG. 12. Energy dependence of the mean longitudinal momentum transfer.

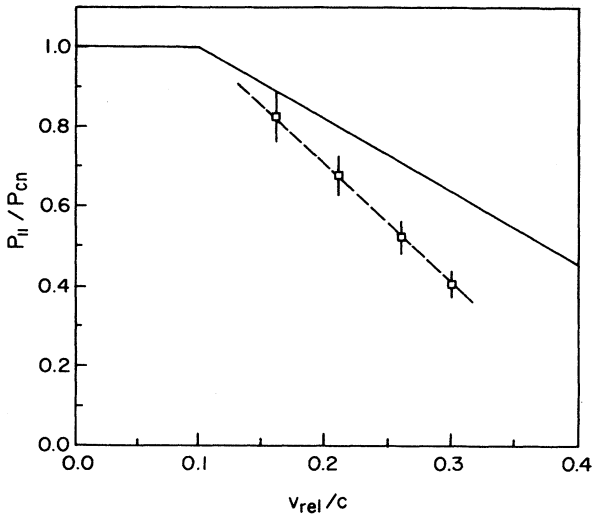

FIG. 13. Variation of the mean fractional longitudinal momentum transfer with relative ion velocity. The solid line is from the Leray systematics. (Ref. 24).

of target and projectile. Figure 13 shows such a plot of the present fractional LMT data along with Leray's fit to other data. While our values do indeed show a linear decrease with increasing relative velocity, a steeper dropoff than that given by Leray is obtained.

E. Excitation energy of residual nuclei

The excitation energy deposited in the struck nucleus by the projectile determines its subsequent deexcitation. Furthermore, various calculations predict the occurrence of limiting values to the excitation energy and nuclear temperature. When these values are reached, the nucleus may undergo multifragmentation.[27–30] Since this limit may be attainable in intermediate-energy heavy-ion reactions, the determination of the excitation energy is of interest.

There are two independent methods for the determination of the mean excitation energy $\langle E^* \rangle$ from the present data, namely, on the basis of the mass yield distributions and on that of the momentum transfer results. Both approaches involve various assumptions so that agreement between them, if it occurs, makes the results more believable.

Values of $\langle E^* \rangle$ were obtained from the mass yield data by use of the code EVA, which calculates the mass distribution resulting from the deexcitation of excited nuclei by the evaporation of nucleons and light particles.[31] For each bombarding energy, we assumed a composite system determined by the value of $\langle \Delta m \rangle$ (Fig. 10). The excitation energy of this nucleus was adjusted to fit the experimental value of the mean product mass number (Fig. 6). In reality, of course, there must be a distribution of composite systems with a distribution of excitation energies. However, calculations based on assumed distributions indicate that the results for the mean product mass are insensitive to reasonable distributions in these quantities. The resulting values of $\langle E^* \rangle$ are plotted versus pro-

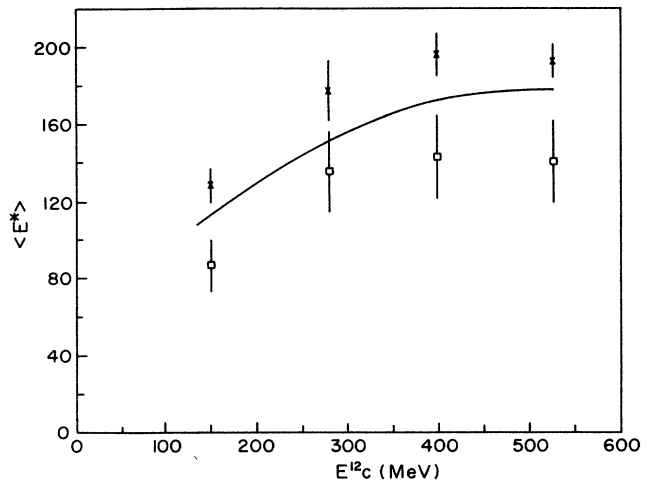

FIG. 14. Dependence of the mean excitation energy of the composite system on ^{12}C energy. Crosses are derived from yield data; open circles are derived from LMT data.

jective energy in Fig. 14. The uncertainty reflects primarily the standard deviation in the mass distribution of products at a given excitation energy.

The mean excitation energy can also be obtained from the values of Δm and hence from those of $v_{\parallel}$. The excitation energy is derived from the total energy of the captured nucleons. Following Leray,[24] we assume that Δm is emitted in the form of free nucleons when calculating Q values for the formation of the composite system. The resulting values of $\langle E^* \rangle$ are plotted in Fig. 14 and are seen to be uniformly lower than those derived from the mean mass loss. While we cannot point to a definite reason for this discrepancy, it may be noted that our mean LMT values are lower than those measured in other experiments (Fig. 13). Thus the $\langle E^* \rangle$ values must also be lower.

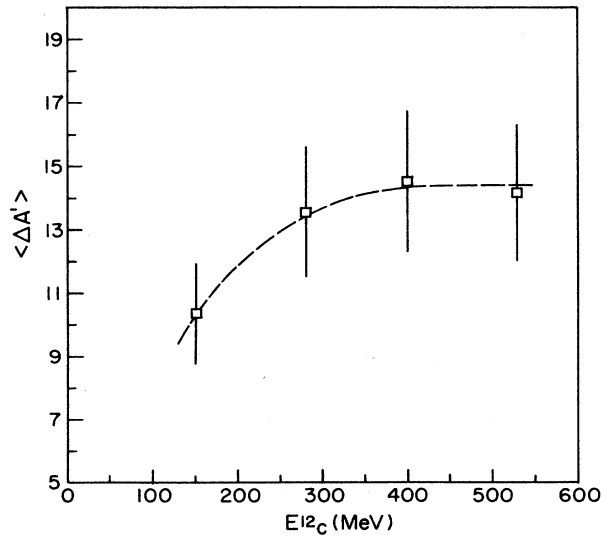

FIG. 15. Energy dependence of the mean mass loss from the composite system, $\langle \Delta A' \rangle$.

In spite of this discrepancy, both sets of $\langle E^* \rangle$ values show that the mean excitation energy first increases with bombarding energy and then levels off. At first sight, the nearly constant values of $\langle E^* \rangle$ at the higher energies appear to be inconsistent with the observed energy dependence of the mass loss from the target (Fig. 6) and with that of the slope of the mass yield distribution (Fig. 7), both of which suggest a monotonic increase in $\langle E^* \rangle$. It must be noted, however, that the mass loss is determined both by the excitation energy and by the mass of the composite system. A better measure of the expected energy dependence of $\langle E^* \rangle$ than given in Fig. 6 is provided by the mean mass loss from the composite system, $\langle \Delta A' \rangle$, plotted in Fig. 15. Owing to the decrease with energy in the mass of the composite system (Fig. 10), the mass loss from this system becomes virtually independent of energy at the higher energies, in accord with the observed dependence of $\langle E^* \rangle$ depicted in Fig. 14.

The constancy of $\langle E^* \rangle$ at the higher energies may reflect the increasing transparency of nuclei for projectiles in the energy regime in question. At even higher energies, where inelastic nucleon-nucleon collisions become important, the excitation energy presumably resumes its increase with bombarding energy until the regime of limiting fragmentation is reached. The data in Fig. 7 support this point of view since the slope of the mass yield curve, which is a measure of the excitation energy, does not level off until a projectile energy of 2–3 GeV is attained.

V. CONCLUSIONS

We have studied the interaction of copper with 15–45 A MeV ^{12}C ions. The isobaric yield distribution remains essentially unchanged in this regime while the mass yield distribution changes substantially: with increasing energy the distribution broadens and the peak moves to lower mass numbers; the mean mass loss from the target increases from approximately 1 to 10 u.

The mean longitudinal momentum transfer (LMT) attains a maximum value of 1.7 ± 0.1 GeV/c at 25 A MeV and decreases at higher energies. The fractional LMT decreases continuously from approximately 0.8 at the lowest energy to 0.4 at the highest one. The mean excitation energy is estimated both from the mass yield distribution and the LMT values. The mean excitation energy initially increases with energy but appears to level off at the higher energies.

ACKNOWLEDGMENTS

We wish to thank Dr. R. Ronningen and the other members of the National Superconducting Cyclotron Laboratory (NSCL) staff for their assistance and cooperation and Dr. B. Glagola for his help with the ATLAS experiment. This work was supported by the U.S. Department of Energy.

[1]J. B. Cumming, R. W. Stoenner, and P. E. Haustein, Phys. Rev. C **14**, 1554 (1976).
[2]J. B. Cumming, P. E. Haustein, and H. C. Hseuh, Phys. Rev. C **18**, 1372 (1978).
[3]G. D. Cole and N. T. Porile, Phys. Rev. C **24**, 2038 (1981).
[4]J. B. Cumming, P. E. Haustein, and H. C. Hseuh, Phys. Rev. C **24**, 2162 (1981).
[5]G. D. Cole and N. T. Porile, Phys. Rev. C **25**, 244 (1982).
[6]T. Lund *et al.*, Phys. Lett. **102B**, 239 (1981).
[7]T. Lund *et al.*, Z. Phys. A **306**, 43 (1982).
[8]A. Lleres, J. Blachot, J. Crancon, A. Gizon, and H. Nifenecker, Z. Phys. A **312**, 177 (1983).
[9]S. Y. Cho, Y. H. Chung, N. T. Porile, and D. J. Morrissey, Phys. Rev. C **36**, 2349 (1987).
[10]L. Kowalski, P. E. Haustein, and J. B. Cumming, Phys. Rev. Lett. **51**, 642 (1983).
[11]N. T. Porile, S. Y. Cho. Y. H. Chung, and D. J. Morrissey, in Third International Conference on Nucleus-Nucleus Collisions, St. Malo, 1988, edited by C. Esteve *et al.* (unpublished).
[12]F. Hubert, A. Fleury, R. Bimbot, and D. Gardes, Ann. Phys. (Paris) **5**, 1 (1980).
[13]T. Routti and S. G. Prussin, Nucl. Instrum. Methods **72**, 125 (1969).
[14]J. B. Cumming, National Academy of Sciences Report NAS-NS-3107, 1962 (unpublished), p. 25.
[15]U. Reus and W. Westmeier, At. Data Nucl. Data Tables **29**, 2 (1983).
[16]G. Rudstam, Z. Naturforsch. **219**, 1027 (1966).
[17]N. T. Porile, G. D. Cole, and C. R. Rudy, Phys. Rev. C **19**, 2288 (1979).
[18]J. B. Cumming, P. E. Haustein, R. W. Stoenner, L. Mausner, and R. A. Neumann, Phys. Rev. C **10**, 739 (1974).
[19]L. G. Sobotka *et al.*, Phys. Rev. Lett. **53**, 2004 (1984).
[20]J. B. Cumming, P. E. Haustein, T. J. Ruth, and G. J. Virtes, Phys. Rev. C **17**, 1632 (1978).
[21]S. Kox *et al.*, Phys. Rev. C **35**, 1678 (1987).
[22]P. J. Karol, Phys. Rev. C **11**, 1203 (1975).
[23]J. B. Cumming, Phys. Rev. Lett. **44**, 17 (1980).
[24]S. Leray, J. Phys. C **4**, 275 (1986).
[25]V. Viola *et al.*, Phys. Rev. C **36**, 178 (1982).
[26]Y. Chan *et al.*, Phys. Rev. C **27**, 447 (1983).
[27]G. Bertsch *et al.*, Phys. Lett. **126B**, 9 (1983).
[28]X. Campi *et al.*, Nucl. Phys. A**428**, 327c (1984).
[29]J. P. Bondorf *et al.*, Nucl. Phys. A**443**, 321 (1985).
[30]D. H. E. Gross *et al.*, Phys. Rev. Lett. **56**, 1544 (1986).
[31]I. Dostrovsky, Z. Fraenkel, and G. Friedlander, Phys. Rev. **116**, 683 (1959).
[32]L. Winsberg, Nucl. Instrum. Methods **150**, 465 (1978).